

# Optimizing Image Retrieval with an Extended $b$ -Metric Space

Abdelkader Belhenniche\*  and Roman Chertovskih 

SYSTEC-ARISE Research Center for Systems and Technologies, Faculty of Engineering, University of Porto, Rua Dr. Roberto Frias s/n, 4200-465, Porto, Portugal; belhenniche@fe.up.pt(A.B.), roman@fe.up.pt(R.C.)

\* Correspondence: belhenniche@fe.up.pt.

**Abstract:** This article provides a new approach on how to enhance data storage and retrieval in the Query By Image Content Systems (QBIC) by introducing the  $NEM_\sigma$  distance measure, satisfying the relaxed triangle inequality. By leveraging the concept of extended  $b$ -metric spaces, we address complex distance relationships, thereby improving the accuracy and efficiency of image database management. The use of  $NEM_\sigma$  facilitates better scalability and accuracy in large-scale image retrieval systems, optimizing both the storage and retrieval processes. The proposed method represents a significant advancement over traditional distance measures, offering enhanced flexibility and precision in the context of image content-based querying. Additionally, we take inspiration from ice flow models like  $NEM_\sigma$  and  $NEM_r$ , adding dynamic and location-based factors to better capture details in images.

**Keywords:** pattern matching; extended  $b$ -metric space; relaxed triangle inequality

**MSC:** 68T10, 45E50, 54E35

## 1. Introduction

A key challenge driving the research presented in this article is the problem of efficient management of data storage and retrieval, particularly digital images, from databases using the Query by Image Content (QBIC) system [1]. The main issue lies in establishing a mathematical framework that enhances the performance of such systems. Some of the methods that evaluate how well human perceptual differences are matched can be found in [2], while a non-linear elastic matching (NEM) distance measure was introduced in [3].

The work of [4] design the NEM distance to compare two ordered sets of contour points,  $A = \{a_1, a_2, \dots, a_m\}$  and  $B = \{b_1, b_2, \dots, b_n\}$ , by establishing a correspondence  $f$  between the points such that the order is preserved. For each correspondence, a stretch  $s(a_i, b_j)$  is assigned based on whether adjacent points in one set align with points in the other. The NEM distance is then computed as the minimum, in all possible correspondences, of the sum of the stretch values and the angular differences  $d(a_i, b_j)$  between the tangent angles at the corresponding points. Dynamic programming techniques are used for this computation. However, this measure does not satisfy neither the triangle inequality nor the relaxed triangle inequality, leading to inaccurate distance estimates and potential errors in pattern matching.

To overcome this limitation, an updated version of NEM, known as  $NEM_r$  (where  $r$  is a positive constant), was developed in [3] and nowadays has been widely used in QBIC systems – a database system that can handle images for pattern matching. This revised method involves stretching the NEM distance by a factor of  $r$  and adding it to the original distance, ensuring that the two boundaries align. Importantly,  $NEM_r$  satisfies the relaxed triangle inequality for any value of  $r$  and within a bounded set  $S$ .

In order to highlight the relevance of the relaxed triangle inequality (not related to pattern matching), we provide the following example (see Figure 1(a)). There are three



**Citation:** Belhenniche A.; Chertovskih R. . Optimizing image retrieval. *Axioms* 2024, 1, 0. <https://doi.org/>

Received:

Revised:

Accepted:

Published:



**Copyright:** © 2024 by the authors. Licensee MDPI, Basel, Switzerland. This article is an open access article distributed under the terms and conditions of the Creative Commons Attribution (CC BY) license (<https://creativecommons.org/licenses/by/4.0/>).

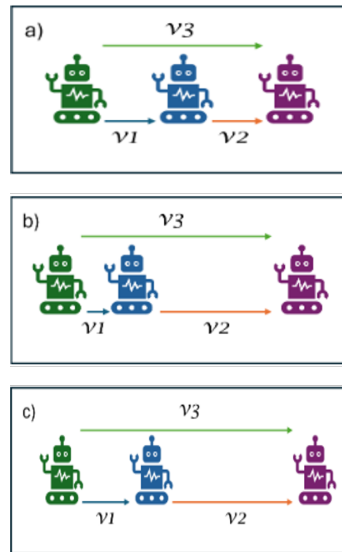


**Figure 1.** Pattern matching with relaxed triangle inequality. (a) represents the three robots in a stable, stationary state, while in (b) and (c) the robots are in motion.

robots (green, blue, and purple ones), placed in space on one straight line. The robots are represented by their shapes, and the distance between them is measured as the minimal distance between their boundaries. While the distance ( $v_1$ ) from the green robot to the blue one and the distance ( $v_2$ ) from the blue robot to the purple are small, the distance from the green robot to the purple one is larger (because it also measures the size of the blue robot), i.e.

$$\begin{aligned} \text{NEM}(\text{Green Robot, Blue Robot}) + \text{NEM}(\text{Blue Robot, Purple Robot}) \\ < \text{NEM}(\text{Green Robot, Purple Robot}). \end{aligned}$$

Note that the sign in the inequality is opposite to the sign in the classical triangle inequality, so NEM is not even satisfy the conditions to be a metric distance. To overcome this, we may consider the  $\text{NEM}_r$  measure, which is a weaker form of the NEM-distance above and satisfies the following relaxed triangle inequality:

$$\begin{aligned} \text{NEM}_r(\text{Green Robot, Purple Robot}) \leq \\ c(\text{NEM}_r(\text{Green Robot, Blue Robot}) + \text{NEM}_r(\text{Blue Robot, Purple Robot})) \end{aligned} \quad (1)$$

for a constant  $c > 1$ .

This approach aligns well with the theoretical foundation of  $b$ -metric spaces. Introduced in the seminal works [5] and [6], and later studied in [7], the  $b$ -metric relaxes the traditional triangle inequality and extends the Banach contraction mapping theorem. Formally, the concept of a  $b$ -metric space can be described as follows:

**Definition 1** ([8,9]). Let  $X$  be a non empty set, and let  $s \geq 1$  be a given real number. A functional  $d : X \times X \rightarrow [0, \infty)$  is said to be a  $b$ -metric if the following conditions are satisfied:

1.  $d(x, y) = 0$  if and only if  $x = y$ ,
2.  $d(x, y) = d(y, x)$ ,
3.  $d(x, z) \leq s[d(x, y) + d(y, z)]$ ,

for all  $x, y, z \in X$ . A pair  $(X, d)$  is called a  $b$ -metric space.

Numerous fixed-point theorems have been developed and their applications thoroughly investigated, in the studies [8–12].

**Example 2 ([12]).** Let  $(X, d)$  be a metric space, and  $\rho(x, y) = (d(x, y))^p$ , where  $p \geq 1$  is a real number. Then,  $(X, \rho)$  is a  $b$ -metric space with  $s = 2^{p-1}$ .

It is clear that a  $b$ -metric space becomes a metric space if we take  $s = 1$ . This clearly shows that the class of  $b$ -metric spaces is larger than that of metric spaces.

In this context, the use of a  $b$ -metric space becomes essential, as it has been explored extensively in various studies. For example, in [13], the authors focused on calculating the dissimilarity ratio between a given image and samples from the IBM QBIC database. They proposed methods for retrieving the most similar shape based on this ratio. Subsequently, numerous studies have emerged that address the calculation of this ratio for different forms of dissimilarity [4].

In [14], the notion of an extended  $b$ -metric space was introduced as a significant generalization of the standard  $b$ -metric space, offering a broader framework for analysis. To formalize this concept, the following definition is presented:

**Definition 3.** Let  $X$  be nonempty, and  $\theta: X \times X \rightarrow [1, +\infty)$ . A function  $b_\theta: X \times X \rightarrow [0, +\infty)$  is an extended  $b$ -metric if, for all  $x, y, z \in X$ , it satisfies:

- 1)  $b_\theta(x, y) = 0$  if and only if  $x = y$
- 2)  $b_\theta(x, y) = b_\theta(y, x)$
- 3)  $b_\theta(x, z) \leq \theta(x, z)[b_\theta(x, y) + b_\theta(y, z)]$

The pair  $(X, b_\theta)$  is called extended  $b$ -metric space.

Denote the open ball (the closed ball, respectively) of radius  $r > 0$  about  $x$  as the set:

$$B_r(x) = \{x \in X: b_\theta(x, y) < r\}, \quad (B_r[x] = \{x \in X: b_\theta(x, y) \leq r\}).$$

**Remark 4.** If  $\theta(x, y) = s$  for  $s \geq 1$ , then  $(X, b_\theta)$  satisfies the definition of a  $b$ -metric space.

**Example 5.** Let  $X = [0, +\infty)$ , and mappings  $b_\theta$  and  $\theta$  with  $\theta: X \times X \rightarrow [1, +\infty)$ , defined by  $b_\theta(x, y) = (x - y)^2$  and  $\theta(x, y) = x + y + 2$ . Then,  $(X, b_\theta)$  is an extended  $b$ -metric space.

**Example 6.** Let  $X = C([a, b], \mathbb{R})$  be the space of all continuous real valued functions defined on  $[a, b]$ . Let  $b_\theta(x, y) = \sup_{t \in [a, b]} \{\|x(t) - y(t)\|^2\}$ , and  $\theta: X \times X \rightarrow [1, +\infty)$  defined by

$$\theta(x, y) := \|x(t)\| + \|y(t)\| + 2,$$

then  $(X, b_\theta)$  is a complete extended  $b$ -metric space.

**Definition 7.** Let  $(X, b_\theta)$  be an extended  $b$ -metric space.

- (i) A sequence  $\{x_n\}_{n \in \mathbb{N}}$  in  $X$  converges to  $x \in X$  if, for every  $\varepsilon > 0$ , there exists  $N = N(\varepsilon) \in \mathbb{N}$  such that

$$b_\theta(x_n, x) < \varepsilon$$

for all  $n \geq N$ . Alternatively we may write  $\lim_{n \rightarrow \infty} x_n = x$ .

- (ii) A sequence  $\{x_n\}_{n \in \mathbb{N}}$  in  $X$  is Cauchy, if for every  $\varepsilon > 0$ , there exists  $N = N(\varepsilon) \in \mathbb{N}$  such that

$$b_\theta(x_m, x_n) < \varepsilon,$$

for all  $m, n \geq N$ .

**Definition 8.** An extended  $b$ -metric space  $(X, b_\theta)$  is complete if every Cauchy sequence in  $X$  is convergent.

An extended  $b$ -metric space does not necessarily satisfy the Hausdorff property. To illustrate this, consider the following example:

**Example 9.** [15] Let  $X = [0, +\infty)$ ,  $\theta: X \times X \rightarrow [1, +\infty)$ ,  $b_\theta(x, y) = (x - y)^2$ , and  $\theta(x, y) = x + y + 2$ . It is evident that  $(X, b_\theta)$  constitutes an extended  $b$ -metric space. However, this space is not Hausdorff, as there are no  $r, r' > 0$  such that:

$$B_r(x) \cap B_{r'}(y) = \emptyset.$$

In fact, the open ball  $B_r(x)$  is contained in  $[0, \sqrt{r} + |z|)$ , and  $B_{r'}(y)$  is contained in  $[0, \sqrt{r'} + \|z'\|)$ . Consequently,

$$B_r(x) \cap B_{r'}(y) \neq \emptyset \quad \forall z, z' \in X.$$

In [16], the authors derive fixed point results in an extended  $b$ -metric space to extend the applicability of fixed point theory to a broader range of real-life problems. They demonstrate that this framework offers a straightforward and efficient solution for Fredholm integral equations within the context of the extended  $b$ -metric space. In [17], the authors introduce and establish various approaches related to the F-contraction by defining new types of contractions, namely the extended FBe-contraction, the extended FBe-expanding contraction, and the extended generalized FBe-contraction. Building on these results, they propose a simple and efficient solution for nonlinear integral equations using the fixed point technique within the framework of a Be-metric space. Additionally, to clarify the conceptual depth of this approach, they provide illustrative examples where necessary.

In [18], the authors define extended suprametric spaces and establish the contraction principle using elementary properties of the greatest lower bound, departing from the traditional iteration procedure. Building on this foundation, they derive topological results and a Stone-type theorem within the framework of suprametric spaces. Moreover, they demonstrate that every suprametric space is metrizable. Further, they prove the existence of solutions to Ito-Doob type stochastic integral equations using their main fixed point theorem in extended suprametric spaces.

Zaslavski’s recent results in fixed-point theory [19], particularly his generalizations of F-contractions and set-valued contractions, offer significant theoretical underpinnings for our approach. These developments are particularly relevant in justifying the use of the relaxed triangle inequality within the NEM measure, which enhances the accuracy and robustness of pattern matching in Query by Image Content systems.

As a continuation of this line of research, [20] introduced an approach by incorporating additional information into the boundary matching process between two shapes. The new dissimilarity measure,  $NEM_{\sigma(x,y)}$ , where  $\sigma: X \times X \rightarrow [0, +\infty)$ , takes into account variable sampling points, and enable computation of distances without the need of fixed starting points on the boundaries of the shapes. Importantly, this measure satisfies the relaxed triangle inequality, i.e.

$$NEM_{\sigma(x,z)}(x, z) \leq \theta(x, z) \left( NEM_{\sigma(x,y)}(x, y) + NEM_{\sigma(y,z)}(y, z) \right), \quad \forall x, y, z \in X, \quad (2)$$

where  $\theta(\cdot, \cdot)$  is a function.

Let us consider the scenario illustrated in Figure 1 (b) and (c): if the robots move with variable velocities, but stay on the same line as in (a). As the three objects come closer and leave each other, the distances between them become a complex function of their initial positions. The relaxed triangle inequality (2) still holds, but now it depends on a function  $\theta(\cdot, \cdot)$ , reflecting the velocities of the objects. Additionally, due to the significant amount of supplementary information required for accurate stretching analysis, we employ a function  $\sigma(\cdot, \cdot)$  rather than relying solely on the simple distance measure  $r$ .

## 2. Application of an extended $b$ -metric space in pattern matching

In what follows we demonstrate how to use an extended  $b$ -metric space for pattern matching. Matching two sequences is, by definition, finding the minimal combined cost-

sum of the stretch and distance cost. First, let us recall the concept of subdividing a segment, which is essential for defining the edges used in the matching process. Consider a compact interval  $[1, n]$ . A subdivision of  $[1, n]$  is a finite set of real numbers:

$$P = \{x_0, x_1, \dots, x_n\},$$

where  $1 = x_0 < x_1 < \dots < x_n = n$ . These subdivisions divide the interval into smaller subintervals, which we define as:

$$I_1 = [x_0, x_1], \quad I_2 = [x_1, x_2], \quad \dots, \quad I_n = [x_{n-1}, x_n].$$

The length of each subinterval  $[x_{i-1}, x_i]$  is denoted by  $\delta x_i = x_i - x_{i-1}$ . This process allows us to break down the intervals into discrete components for comparison.

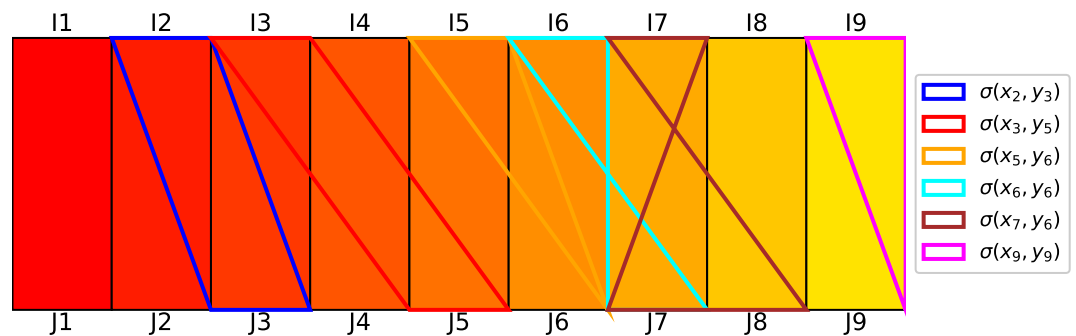


**Figure 2.** Minimal (9,9)- $\sigma$ -mapping with the stretch cost of  $\sigma(x_2, y_3) + \sigma(x_3, y_5) + \sigma(x_5, y_6) + \sigma(x_6, y_6) + \sigma(x_7, y_6) + \sigma(x_9, y_9)$ .

Next, we consider two compact intervals,  $[1, m]$  and  $[1, n]$ , which have both been subdivided. An  $(m, n)$ - $\sigma$ -mapping is a set  $M \subseteq [1, m] \times [1, n]$ . Each pair  $\langle I_i, J_i \rangle \in M$  is called a  $\delta$ -edge if it satisfies the following conditions:

1. Every subdivision in  $[1, m]$  is the first component  $I_i$  of some  $\delta$ -edge  $\langle I_i, J_i \rangle \in M$ .
2. Every subdivision in  $[1, n]$  is the second component  $J_i$  of some  $\delta$ -edge  $\langle I_i, J_i \rangle \in M$ .
3. There do not exist  $I_i, I'_i, J_i, J'_i$  with  $\delta x_i < \delta x'_i$  and  $\delta y_i < \delta y'_i$  that would violate the ordering.

A  $\delta$ -edge is a  $\sigma$ -stretch-edge if both  $\langle I_{i-1}, J_i \rangle$  and  $\langle I_i, J_{i-1} \rangle$  are present in  $M$ .

For each  $\delta$ -edge  $\langle I_i, J_i \rangle \in M$ , we define two types of costs:

- The stretch cost or  $s$ -cost, denoted by  $s\text{-cost}(\langle I_i, J_i \rangle, M)$ , measures how much the pattern is stretched during matching. It is defined as:

$$s\text{-cost}(\langle I_i, J_i \rangle, M) = \begin{cases} \sigma(x_i, y_j), & \text{if } \langle I_i, J_i \rangle \text{ is a } \sigma\text{-stretch-edge,} \\ 0, & \text{otherwise.} \end{cases}$$

For instance, in Figure 2, the minimal (9,9)- $\sigma$ -mapping is depicted, highlighting specific  $\delta$ -edges as  $\sigma$ -stretch edges. The  $\sigma$ -stretch edges include  $\langle I_2, J_3 \rangle, \langle I_3, J_5 \rangle, \langle I_5, J_6 \rangle, \langle I_6, J_6 \rangle, \langle I_7, J_6 \rangle$ , and  $\langle I_9, J_9 \rangle$ . The total cost associated with these  $\sigma$ -stretch edges is given by  $\sigma(x_2, y_3) + \sigma(x_3, y_5) + \sigma(x_5, y_6) + \sigma(x_6, y_6) + \sigma(x_7, y_6) + \sigma(x_9, y_9)$ . All other  $\delta$ -edges in the mapping are associated with a stretch cost of zero.

- The distance cost, denoted by  $d\text{-cost}(\langle I_i, J_i \rangle)$ , measures the distance between corresponding subdivisions, i.e.  $d\text{-cost}(\langle I_i, J_i \rangle) = b(x_i, y_j)$ , where  $b(x_i, y_j)$  represents the cost associated with aligning segment  $I_i$  from sequence  $x$  with segment  $J_j$  from sequence  $Y$ . This measure captures various alignment challenges, including shape deformation, feature mismatches, and other discrepancies. By quantifying these alignment costs,  $b(x_i, y_j)$  provides a flexible and comprehensive way to evaluate how well different segments of sequences fit together, making it an essential component of extended  $b$ -metric spaces.

### Total Cost of the $(m, n)$ - $\sigma$ -Mapping

The total cost of the  $(m, n)$ - $\sigma$ -mapping  $M$  is the sum of two components: the stretch cost and the distance cost. Let us define these costs more precisely.

The total stretch cost is given by the double integral over the stretch function  $\sigma(x_i, y_j)$ , which represents the stretching penalty when matching the elements  $x_i$  and  $y_j$ . It is expressed as:

$$\sum_{i=0}^m \sum_{j=0}^n \int_{x_i} \int_{y_j} \sigma(x_i, y_j) dx_i dy_j,$$

where  $\sigma(x_i, y_j)$  represents how much  $x_i$  has to be stretched to match  $y_j$ .

The **total distance cost** is given by the double integral over the distance function  $b(x_i, y_j)$ , which quantifies the distance between  $x_i$  and  $y_j$ . This cost is expressed as:

$$\sum_{i=0}^m \sum_{j=0}^n \int_{x_i} \int_{y_j} b(x_i, y_j) dx_i dy_j.$$

Thus, the overall total cost of the mapping  $M$ , denoted as  $Cost(M, x, y)$ , is the sum of both the stretch and distance costs:

$$Cost(M, x, y) = \sum_{i=0}^m \sum_{j=0}^n \int_{x_i} \int_{y_j} \sigma(x_i, y_j) dx_i dy_j + \sum_{i=0}^m \sum_{j=0}^n \int_{x_i} \int_{y_j} b(x_i, y_j) dx_i dy_j.$$

### Normalized Extended Matching Cost

The normalized extended matching cost, denoted by  $NEM_{\sigma(x,y)}$ , is the minimum total cost over all possible  $(m, n)$ - $\sigma$ -mappings  $M$ . That is,

$$NEM_{\sigma(x,y)}(x, y) = \min_M Cost(M, x, y).$$

This normalized cost represents the optimal matching cost between the sequences  $x$  and  $y$ , considering both the stretch and distance costs. In other words,  $NEM_{\sigma(x,y)}$  captures the minimal cost required to align the sequences  $x$  and  $y$  under the given  $\sigma$ -mapping, taking into account all possible pairings of elements from the two sequences.

### Properties of the Normalized Extended Matching Cost

#### Symmetry

The first property to verify is symmetry. For any two sequences  $x$  and  $y$ , the symmetry of the matching cost is evident. Both the stretch cost and the distance cost are symmetric functions. Specifically, the distance cost function  $b(x_i, y_j)$  satisfies  $b(x_i, y_j) = b(y_j, x_i)$ , and the stretch cost  $\sigma(x_i, y_j)$  is also symmetric. Therefore, the total cost associated with matching  $x$  to  $y$  is identical to matching  $y$  to  $x$ . This gives us:

$$NEM_{\sigma(x,y)}(x, y) = NEM_{\sigma(y,x)}(y, x).$$

Thus, the symmetry property of the extended  $b$ -metric space is satisfied.

#### Non-Negativity and Identity of Indiscernibles

Next, we consider non-negativity and the identity of indiscernibles. The non-negativity follows from the fact that both the stretch cost and the distance cost are non-negative. Specifically, since  $\sigma(x_i, y_j) \geq 0$  and  $b(x_i, y_j) \geq 0$  for all pairs  $(x_i, y_j)$ , we can conclude that

$$NEM_{\sigma(x,y)}(x, y) \geq 0.$$

For the identity of indiscernibles, if  $x = y$ , then the distance cost  $b(x_i, y_j)$  becomes zero whenever  $x_i = y_j$ , and the stretch cost  $\sigma(x_i, y_j)$  is also zero since no stretching is required. Therefore, if  $x = y$ , we have:

$$\text{NEM}_{\sigma(x,y)}(x, y) = 0.$$

Conversely, if  $\text{NEM}_{\sigma(x,y)}(x, y) = 0$ , this implies that both the stretch cost and the distance cost are zero for all pairs  $(x_i, y_j)$ , which can only occur if  $x = y$ . Thus, we have the identity of indiscernibles property:

$$\text{NEM}_{\sigma(x,y)}(x, y) = 0 \quad \text{if and only if} \quad x = y.$$

*Generalized Triangle Inequality*

Finally, we verify the relaxed triangle inequality. The generalized triangle inequality is given by:

$$\text{NEM}_{\sigma(x,z)}(x, z) \leq \theta(x, z) \left( \text{NEM}_{\sigma(x,y)}(x, y) + \text{NEM}_{\sigma(y,z)}(y, z) \right),$$

where  $\theta(x, z)$  is a positive bounded function. To prove this, we use the fact that the distance cost function satisfies the traditional triangle inequality. Specifically, for the distance cost, we have:

$$b(x_i, z_k) \leq \theta(x_i, z_k) (b(x_i, y_j) + b(y_j, z_k)).$$

Since the stretch cost is additive, the total cost of matching  $x$  to  $z$  is bounded by the sum of the costs of matching  $x$  to  $y$  and  $y$  to  $z$ , scaled by the function  $\theta(x, z)$ . Therefore, the total matching cost satisfies:

$$\text{Cost}(M, x, z) \leq \theta(x, z) (\text{Cost}(M, x, y) + \text{Cost}(M, y, z)).$$

Taking the minimum over all mappings  $M$ , we obtain:

$$\text{NEM}_{\sigma(x,z)}(x, z) \leq \theta(x, z) \left( \text{NEM}_{\sigma(x,y)}(x, y) + \text{NEM}_{\sigma(y,z)}(y, z) \right).$$

Thus, the generalized triangle inequality holds, confirming that  $\text{NEM}_{\sigma(x,y)}$  satisfies the conditions required to be an extended  $b$ -metric space.

**3. Comparison of Ice Flow Patterns:  $\text{NEM}_{\sigma}$  vs  $\text{NEM}_r$**

Synthetic Aperture Radar (SAR) plays a vital role in monitoring ice floe movement in polar regions, offering high-resolution images unaffected by weather conditions or the time of day. This makes SAR particularly effective in the Arctic and Antarctic, where optical images are often obscured by clouds or darkness. The movement of ice floes is significant for weather patterns as it exposes vast areas of unfrozen ocean water to cold Arctic air, influencing heat exchange between the ocean and atmosphere. Additionally, understanding ice floe dynamics is essential for ocean navigation and oil exploration activities.

SAR technology was first introduced by Wiley [21], who demonstrated its potential to generate high-resolution radar images using Doppler shifts. This revolutionary technology has since been widely applied in various fields, including glaciology, oceanography, and topographic studies. Over the years, advancements have focused on automating the mapping of ice floe motion from SAR images, as manual tracking is labor-intensive and time-consuming. One common method for ice floe tracking is area correlation, which matches patches of pixels from one image to another. While effective, this method struggles with issues such as rotating and deformed ice floes and can be computationally expensive.

To overcome these challenges, McConnell et al [22] proposed shape-matching algorithms that integrate rotation and deformation adjustments, improving the accuracy



of tracking by generating motion and rotation vectors. These algorithms use normalized correlation with shape descriptors and dynamic programming for elastic matching, which handles the deformation of ice floes more effectively (see [22–25]). Kwok et al in [26] further advanced ice motion tracking systems, specifically for the Alaska SAR Facility, ensuring high-quality motion detection and analysis.

Building on these foundational works, our study applies elastic matching to simulate ice flow using two models,  $NEM_{\sigma}$  and  $NEM_r$ . Our results highlight the advantages of  $NEM_{\sigma}$  in accurately simulating realistic ice flow patterns and improving the precision of ice motion mapping from SAR imagery.

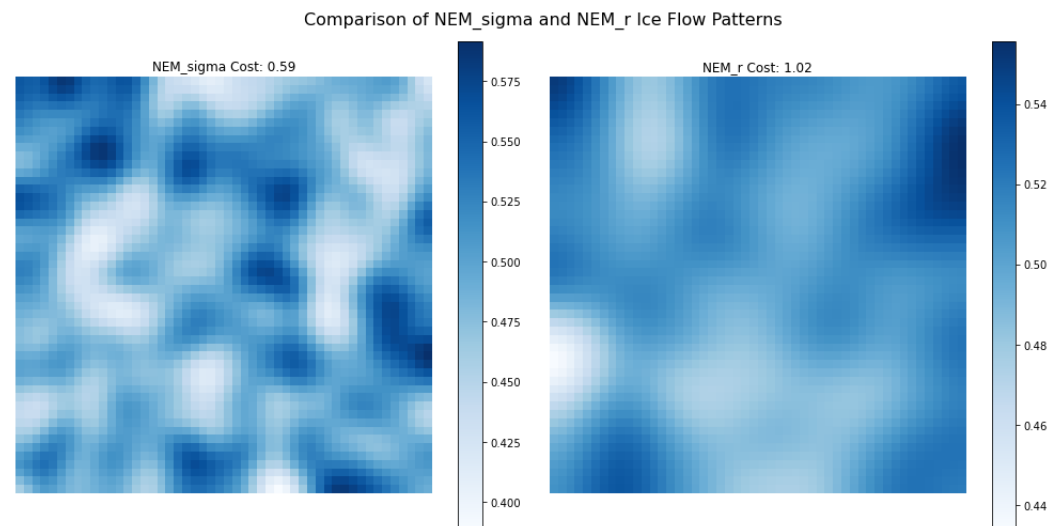


**Figure 3.** Comparison of Ice Flow Patterns Under Different NEM Cost Models:  $NEM_{\sigma}$  versus  $NEM_r$ .

#### 4. Analysis of Ice Flow Patterns: Comparison of Diffusion Models

The distributions of blue and white areas in the simulations represent regions of varying ice intensity. Blue areas correspond to regions of lower "ice intensity" or diffusion in the simulated ice flow, which could indicate thinner or slower-moving ice. White areas, on the other hand, represent regions of higher "ice intensity" or diffusion, potentially indicating thicker or faster-moving ice. The spatial distribution of these regions reflects the heterogeneity of the ice flow patterns, which are influenced by the role of  $\sigma$  or  $r$  in the diffusion process over time. In the  $NEM_{\sigma}$  approach,  $\sigma$  is variable and depends on spatial coordinates and time, introducing characteristics such as localized variations. Regions closer to the center of the grid experience higher values of  $\sigma$ , allowing for faster diffusion and resulting in lighter (white) areas, while regions farther from the center have lower values of  $\sigma$ , leading to slower diffusion and darker (blue) regions. The variable  $\sigma$  adapts to local conditions, such as distance from the center and time modulation, introducing fine-grained, high-frequency variations in the ice flow, which creates a more complex and realistic pattern. In contrast, in the  $NEM_r$  approach,  $r$  is constant across the entire grid, leading to uniform diffusion with smoother distributions and fewer sharp transitions between blue and white regions. This lack of variability in  $r$  fails to capture localized differences in ice flow dynamics, resulting in a less detailed and overly simplified pattern. Comparing the two approaches highlights the superiority of  $NEM_{\sigma}$  in modeling ice flow patterns. The  $NEM_{\sigma}$  approach adapts to localized conditions by allowing  $\sigma$  to vary with spatial and temporal factors, which is crucial for modeling real-world ice flows influenced by heterogeneous factors such as temperature, terrain, and stress. The spatial heterogeneity captured by  $NEM_{\sigma}$  aligns with real-world ice flow behavior, where diffusion rates differ due to environmental variations, whereas  $NEM_r$  oversimplifies this behavior by treating all regions equally. Additionally, the calculated costs show that  $NEM_{\sigma}$  achieves a better fit



with a cost of 0.59, leveraging its flexibility, while  $NEM_r$  incurs a higher cost of 1.02 due to its inability to optimize for localized variations.

## 5. Conclusion

In this article, we have introduced the  $NEM_\sigma$  measure as a novel approach for Query by Image Content systems, leveraging the powerful framework of extended  $b$ -metric spaces. By constructing a distance measure that satisfies a relaxed version of the triangle inequality, we laid the groundwork for more accurate and efficient image retrieval, even in the face of dynamic, variable object velocities. This new measure has the potential to significantly enhance the precision of search results while also improving the scalability and robustness of data management systems. Our findings suggest that  $NEM_\sigma$  could be a transformative tool in the advancement of image retrieval technologies. Moving forward, we aim to empirically validate the effectiveness of  $NEM_\sigma$  in real-world applications, where it could substantially boost the performance of image-based search engines and improve the overall quality of large-scale image datasets handling.

**Funding:** A.B. acknowledges the financial support of the Foundation for Science and Technology (FCT, Portugal) in the framework of the grant 2021.07608.BD. Also, both authors acknowledge the financial support of the FCT in the framework of ARISE (DOI 10.54499/LA/P/0112/2020) and R&D Unit SYSTEC (base UIDB/00147/2020 and programmatic UIDP/00147/2020 funds).

**Author Contributions:** Conceptualization, A.B and R.C.; methodology, A.B; software, A.B. and R.C.; validation, R.C.; formal analysis, A.B. and R.C.; investigation, A.B and R.C.; writing-original draft preparation, A.B; writing-review and editing, R.C; visualization, A.B and R.C; funding acquisition, R.C. All authors have read and agreed to the published version of the manuscript.

**Data Availability Statement:** The datasets analysed in this paper are not readily available due to technical limitations.

**Acknowledgments:** The paper is dedicated to memory of Professor Fernando Manuel Ferreira Lobo Pereira, an outstanding and world-renowned expert in Optimal Control, who passed away in June 2022.

**Conflicts of Interest:** The authors declare no conflicts of interest.

## References

1. Niblack, W.; Barber, R.; Equitz, W.; Flickner, M.; Glasman, E.; Petkovic, D.; Yanker, P. The QBIC project: querying images by content using color, texture, and shape. In *Proceedings of the Conference on Storage and Retrieval for Image and Video Databases*, San Jose, CA, 1993; Volume 1908, pp. 173–181.
2. Scassellati, B.; Alexopoulos, S.; Flickner, M. Retrieving images by 2D shape: a comparison of computation methods with human perceptual judgments. In *Proceedings of the Conference on Storage and Retrieval for Image and Video Databases II*, San Jose, CA, 1994; Volume 2185, pp. 2–14.
3. Niblack, W.; Yin, J. A pseudo-distance measure for 2D shapes based on turning angle. In *Proceedings of the IEEE International Conference on Image Processing*, Washington, DC, 1995.
4. Veltkamp, R. C. Shape matching: similarity measures and algorithms. In *Proceedings of the International Conference on Shape Modeling and Applications, SMI 2001*, IEEE, 2001; pp. 188–197.
5. Bourbaki, N. *Topologie Générale*; Herman: Paris, France, 1974.
6. Bakhtin, I. A. The Contraction Mapping Principle in Almost Metric Spaces. *Functional Analysis and Its Applications* **1989**, *30*, 26–37.
7. Czerwik, S. Contraction Mappings in  $b$ -Metric Spaces. *Acta Mathematica Informatica Universitatis Ostraviensis* **1993**, *1*, 5–11.
8. Bakhtin, I. A. The contraction mapping principle in quasimetric spaces. *Funct. Anal., Unianowsk Gos. Ped. Inst.* **1989**, *30*, 26–37.
9. Czerwik, S. Nonlinear set-valued contraction mappings in  $b$ -metric spaces. *Atti Sem. Mat. Univ. Modena* **1998**, *46*, 263–276.
10. Kirk, W. A.; Sems, B. *Handbook of Metric Fixed-Point Theory*; Kluwer Academic Publishers: Iowa City and Newcastle, 2001.
11. Rao, K. P. R.; Swamy, P. R.; Prasad, J. R. A common fixed-point theorem in complex valued  $b$ -metric spaces. *Bulletin of Mathematics and Statistics Research* **2013**, *1*, 1–9.
12. Roshan, J.; Parvaneh, V.; Sedghi, S.; Shobkolaei, N.; Shatanawai, W. Common fixed-points of almost generalized  $(\psi, \phi)$ -contractive mapping in ordered  $b$ -metric spaces. *Fixed-Point Theory and Applications* **2013**, *159*, 1–10.
13. Fagin, R.; Stockmeyer, L. Relaxing the triangle inequality in pattern matching. *International Journal of Computer Vision* **1998**, *30*, 219–231.
14. Kamran, T.; Samreen, M.; Ul Ain, Q. A generalization of  $b$ -metric space and some fixed point theorems. *Mathematics* **2017**, *5*, 19.

15. Belhenniche, A.; Guran, L.; Benahmed, S.; Lobo Pereira, F. Solving nonlinear and dynamic programming equations on extended  $b$ -metric spaces with the fixed-point technique. *Fixed Point Theory and Algorithms for Sciences and Engineering* **2022**, *2022*, 24.
16. Karapınar, E.; Kumari, P. S.; Lateef, D. A new approach to the solution of the Fredholm integral equation via a fixed point on extended  $b$ -metric spaces. *Symmetry* **2018**, *10*, 512.
17. Panda, S. K.; Tassaddiq, A.; Agarwal, R.P. A new approach to the solution of non-linear integral equations via various FBe-contractions. *Symmetry*, **11**, 2019.
18. Panda, S. K.; Agarwal, R. P.; Karapınar, E. Extended suprametric spaces and Stone-type theorem. *Symmetry* **2023**.
19. Zaslavski, A. J. Three Existence Results in the Fixed Point Theory. *Axioms* **2024**, *13*, 425.
20. Eguia, I.; Lozano, S.; Racero, J.; Guerrero, F. A methodological approach for designing and sequencing product families in reconfigurable disassembly systems. *Journal of Industrial Engineering and Management* **2011**, *4*, 418–435.
21. Wiley, C. A. Synthetic aperture radars. *IEEE Trans. Aerospace Electron. Syst.* **1985**, *3*, 440–443.
22. McConnell, R.; Kober, W.; Leberl, F.; Kwok, R.; Curlander, J. Automated tracking of Arctic ice floes in multitemporal SAR imagery. In *Int. Geosci. Remote Sensing Symp. (IGARSS)*, Vancouver, Canada, July 1989.
23. Daida, J.; Vesecky, J. Object-based feature-tracking algorithms for SAR images of the marginal ice zone. In *Trans. Int. Geosci. Remote Sensing Symp.*, Vancouver, Canada, 1989.
24. Fily, M.; Rothrock, D. A. Extracting sea ice data from satellite SAR imagery. *IEEE Trans. Geosci. Remote Sensing* **1986**, *24*, 849–854.
25. Vesecky, J. F.; Curlander, J.; McConnell, R.; Kwok, R. Observation of sea-ice dynamics using synthetic aperture radar images: automated analysis. *IEEE Trans. Geosci. Remote Sensing* **1987**, *26*, 38–47.
26. Kwok, R.; Curlander, J.; McConnell, R.; Pang, S. An ice motion tracking system at the Alaska SAR Facility. *IEEE J. Oceanic Eng.* **1989**, *15*, 44–54.

**Disclaimer/Publisher’s Note:** The statements, opinions and data contained in all publications are solely those of the individual author(s) and contributor(s) and not of MDPI and/or the editor(s). MDPI and/or the editor(s) disclaim responsibility for any injury to people or property resulting from any ideas, methods, instructions or products referred to in the content.